

# Supporting Information

## Polymer/Perovskite-Type Nanoparticle Multilayers with Multi-Electric Properties Prepared from Ligand Addition-Induced Layer-by-Layer Assembly

Younghoon Kim,<sup>1†</sup> Kyungyun Kook,<sup>1†</sup> Sun Kak Hwang,<sup>2</sup> Cheolmin Park,<sup>2</sup> and Jinhan Cho<sup>1\*</sup>

(Unit: nm)

OA-BTO NPs concentration	1000 rpm	2000 rpm	3000 rpm	4000 rpm
5 mg·mL <sup>-1</sup>	19 ± 5.8	14 ± 1.9	12 ± 1.1	11 ± 0.9
10 mg·mL <sup>-1</sup>	26 ± 4.3	22. ± 3.7	19 ± 1.9	18 ± 1.1
15 mg·mL <sup>-1</sup>	35 ± 4.1	32. ± 2.8	28 ± 2.8	22 ± 2.1
20 mg·mL <sup>-1</sup>	46 ± 4.2	41 ± 1.8	34 ± 2.6	27 ± 2.7
30 mg·mL <sup>-1</sup>	65 ± 4.9	57 ± 3.7	49 ± 3.3	42 ± 3.2

**Table S1.** Thickness data of the single-step spin-coated films as a function of concentration of OA-BTO NP solution and spinning speed.

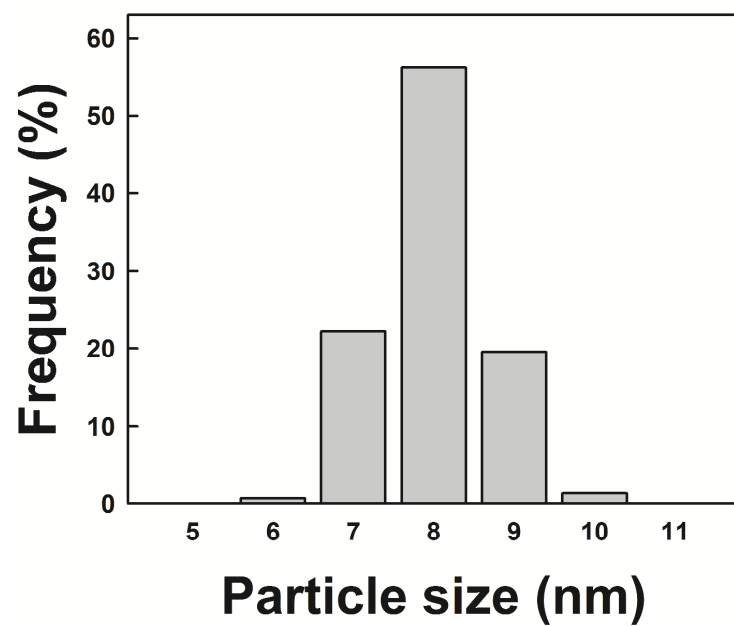


**Figure S1.** The particle size distribution histogram of approximately 8 nm OA-BTO NPs.

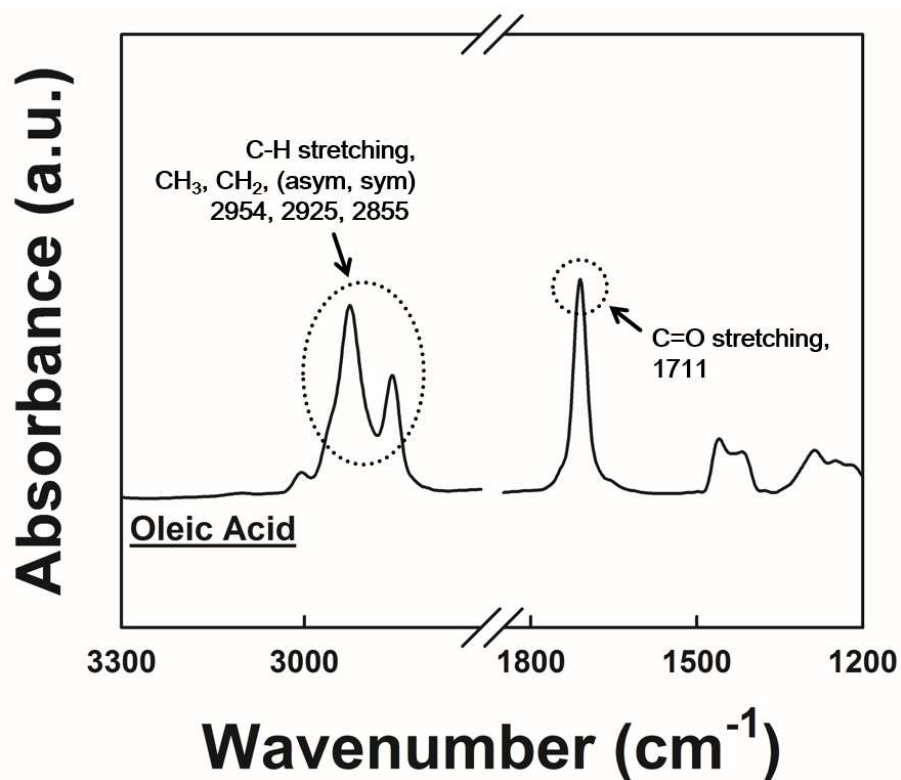


**Figure S2.** FT-IR spectrum of pure oleic acid. The C–H stretching (2855, 2925 and 2954 cm<sup>-1</sup>) and C=O stretching (1711 cm<sup>-1</sup>) peaks contributed to the long aliphatic chains and carboxylic acid (–COOH) groups of the pure oleic acid.

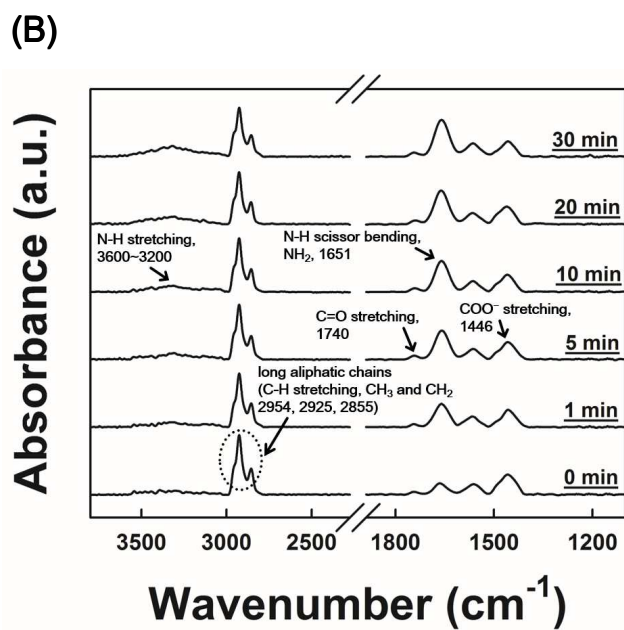
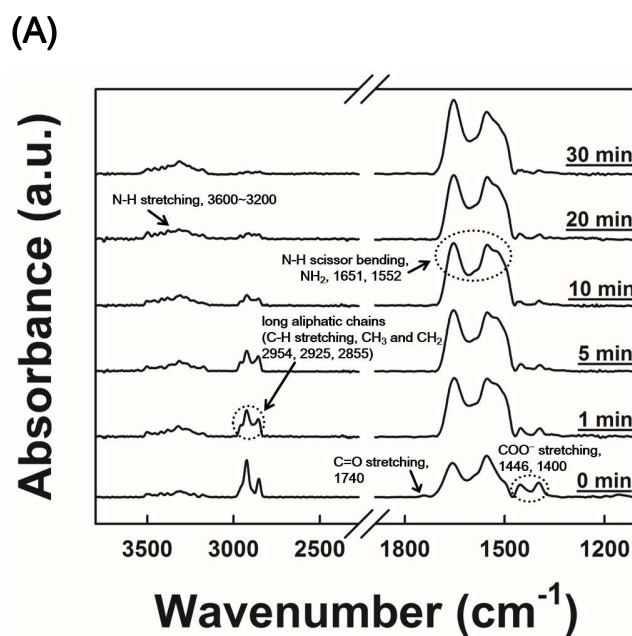


**Figure S3.** FT-IR spectra of LbL-assembled film as a function of adsorption time of the  $\text{NH}_2$ -dendrimer onto (A) the outermost OA-Ag NP layer- and (B) the outermost OA-BTO NP layer-coated films.

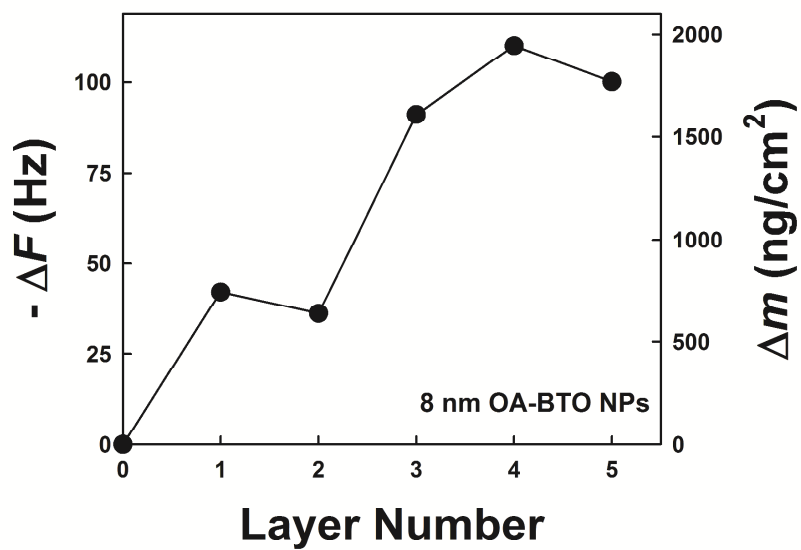


**Figure S4.** (a) QCM analysis of the successive spin-coated (OA-BTO NP)<sub>5</sub> film without an aid of NH<sub>2</sub>-dendrimer layers prepared using the solution concentration of 10 mg·mL<sup>-1</sup> at the spinning speed of 3000 rpm.

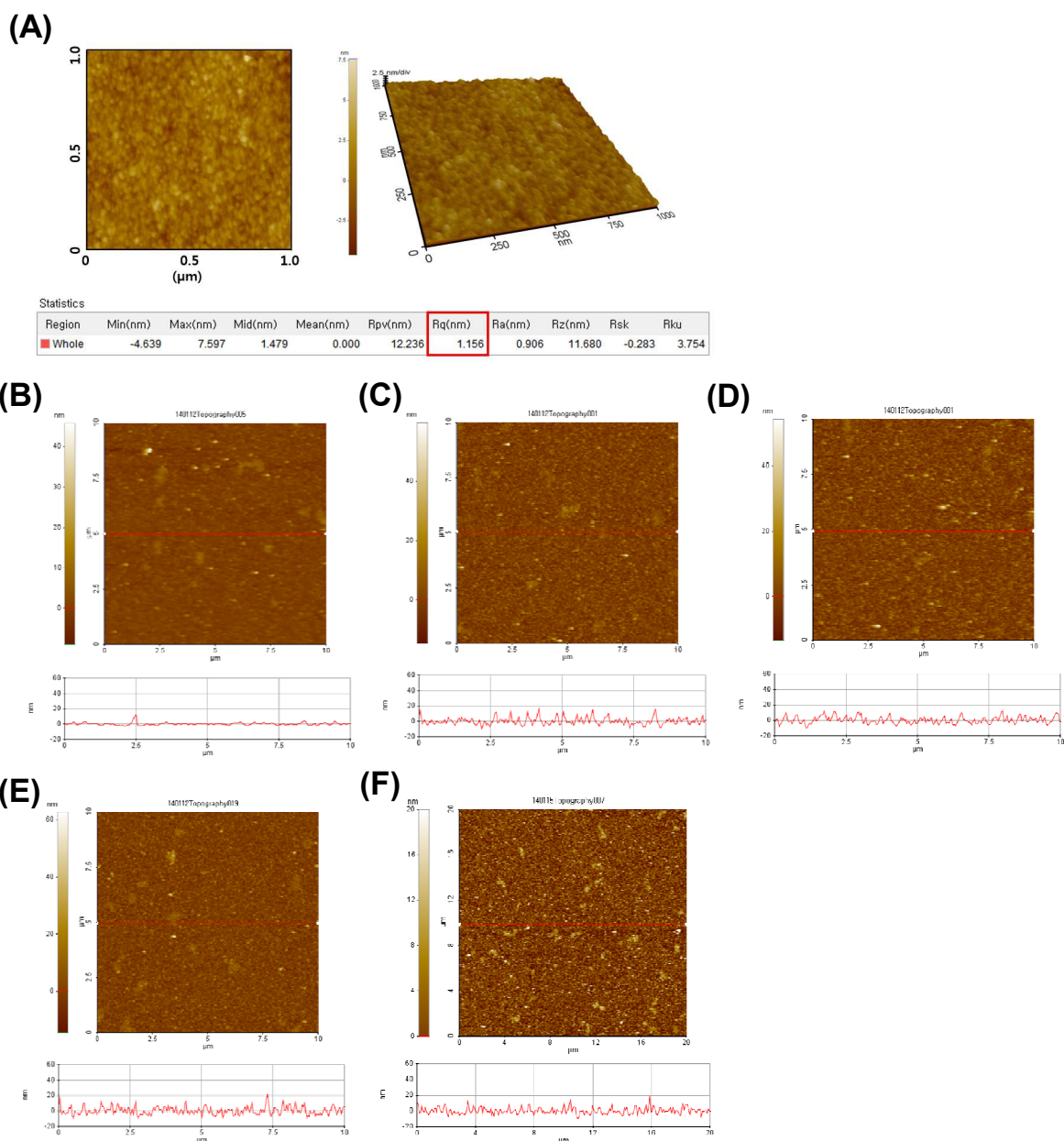


**Figure S5.** (A) AFM images of  $(\text{NH}_2\text{-dendrimer/OA-BTO NP})_5$  multilayer film deposited on a silicon wafer. The root-mean-square (RMS) surface roughness was measured to be about 1.16 nm in the scan area of  $1 \times 1 \mu\text{m}^2$ . (B) – (E) AFM images of the  $(\text{NH}_2\text{-dendrimer/OA-BTO NP})_n$  multilayer films measured in the scan area of  $10 \times 10 \mu\text{m}^2$ . In these cases, the surface roughnesses of multilayers were measured to be (B) about 1.32 nm for  $n = 5$ , (C) 1.86 nm for  $n = 10$ , (D) 1.92 nm for  $n = 15$ , and (E) 2.12 nm for  $n = 20$ . (F) AFM images of the  $(\text{NH}_2\text{-dendrimer/OA-BTO NP})_{20}$  multilayer films measured in the scan area of  $20 \times 20 \mu\text{m}^2$ . The measured RMS surface roughness was measured to be about 2.82 nm.

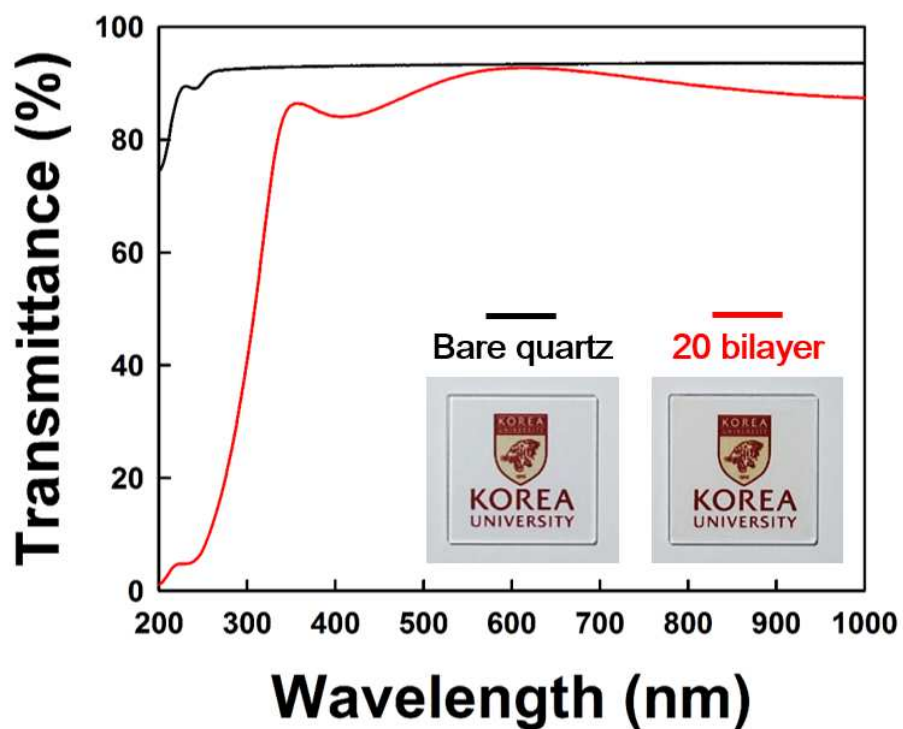


**Figure S6.** Light transmittance curves of the bare quartz substrate and the  $(\text{NH}_2\text{-dendrimer/OA-BTO NP})_{20}$  multilayer-coated quartz substrate. The inset shows photographic images of bare quartz substrate and 20-bilayered BTO nanocomposite film-coated substrate. In this case, the light transmissions of bare and multilayer-coated quartz substrates were measured to be about 93.3 and 92.7 % at the wavelength of 600 nm, respectively.

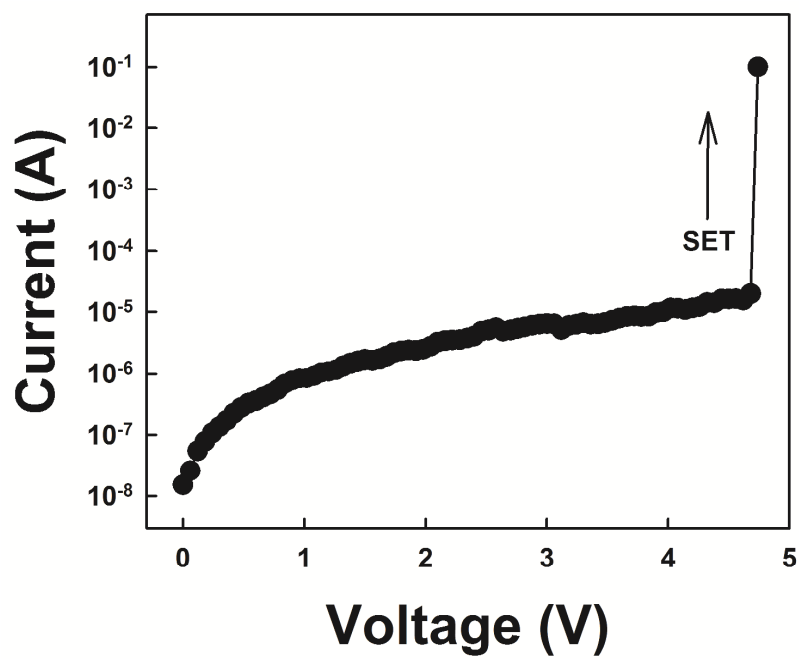


**Figure S7.** Initial electroforming  $I$ - $V$  curve of a 5-bilayered device with a current compliance of 100 mA.

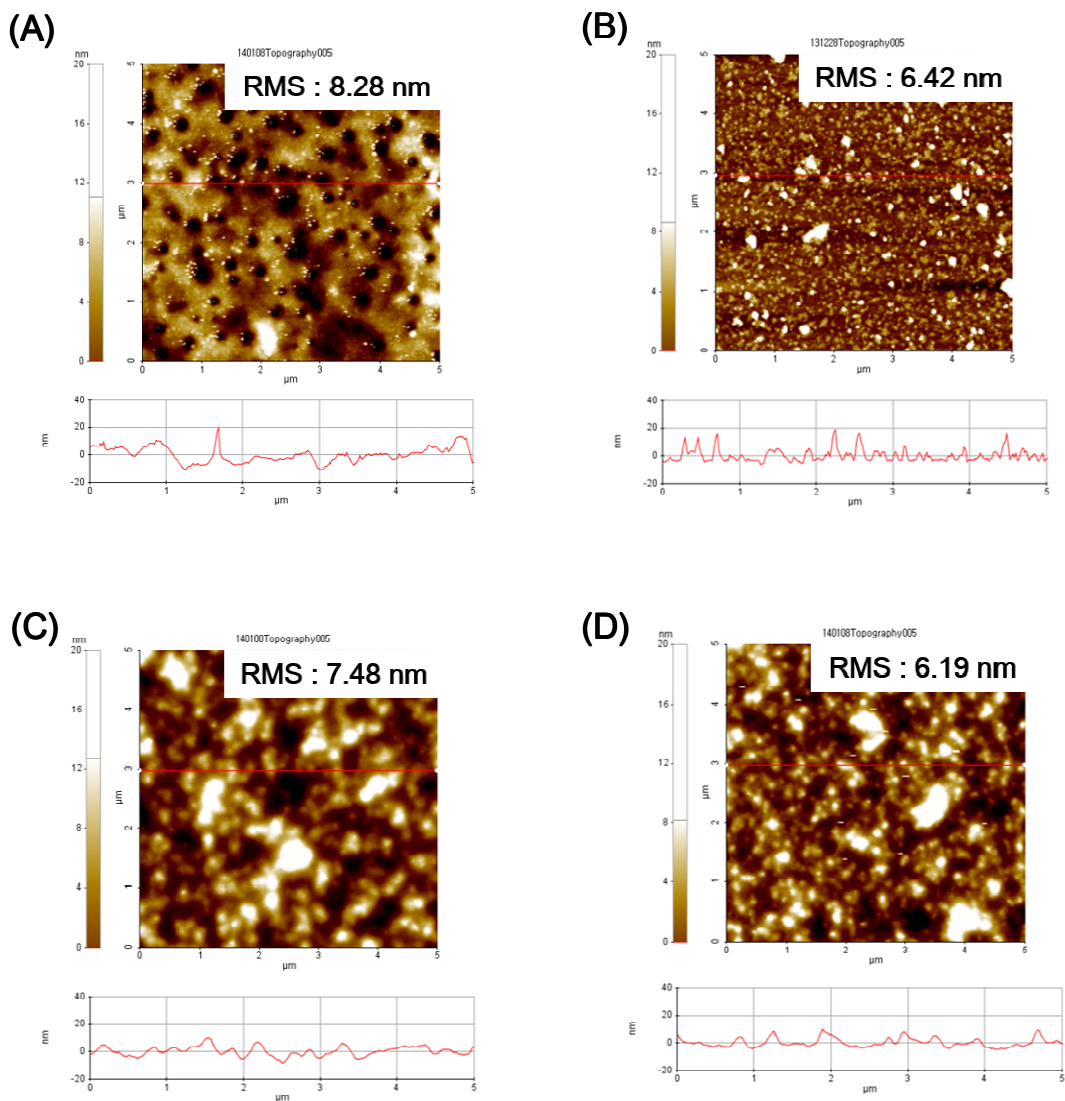


**Figure S8.** (A) AFM topographic image of the simple-casted film prepared using the OA-BTO NP solution concentration of 5 mg·mL<sup>-1</sup>. AFM topographic images of the single-step spin coated films using OA-BTO NP concentrations of (B) 10 mg·mL<sup>-1</sup> at the spinning speed of 3000 rpm, (C) 30 mg·mL<sup>-1</sup> at the spinning speed of 1000 rpm, and (D) 30 mg·mL<sup>-1</sup> at the spinning speed of 3000 rpm.

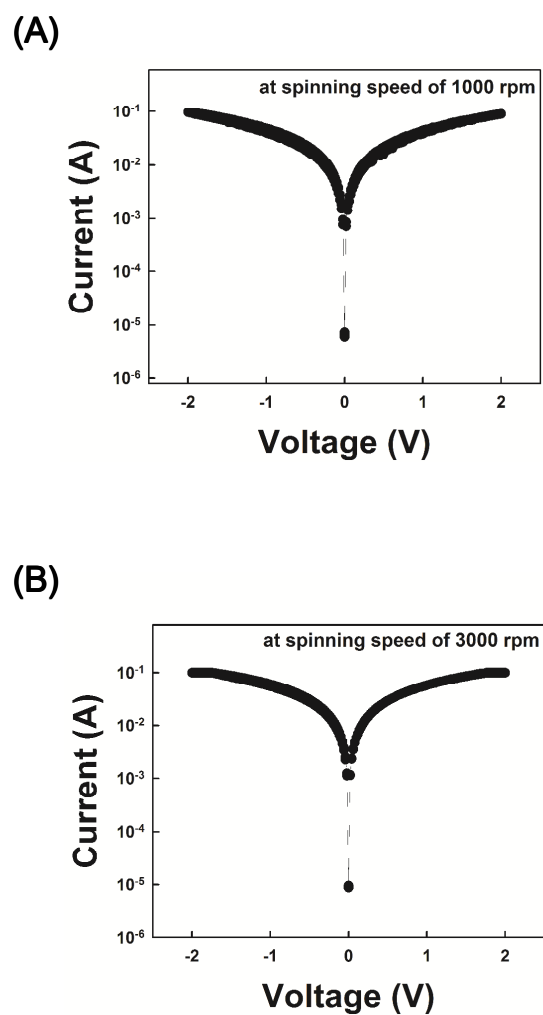


**Figure S9.**  $I$ - $V$  curves of the single-step spin-coated (OA-BTO NP)<sub>1</sub> film prepared using the solution concentration of 30 mg·mL<sup>-1</sup> at the spinning speed of (A) 1000 and (B) 3000 rpm.

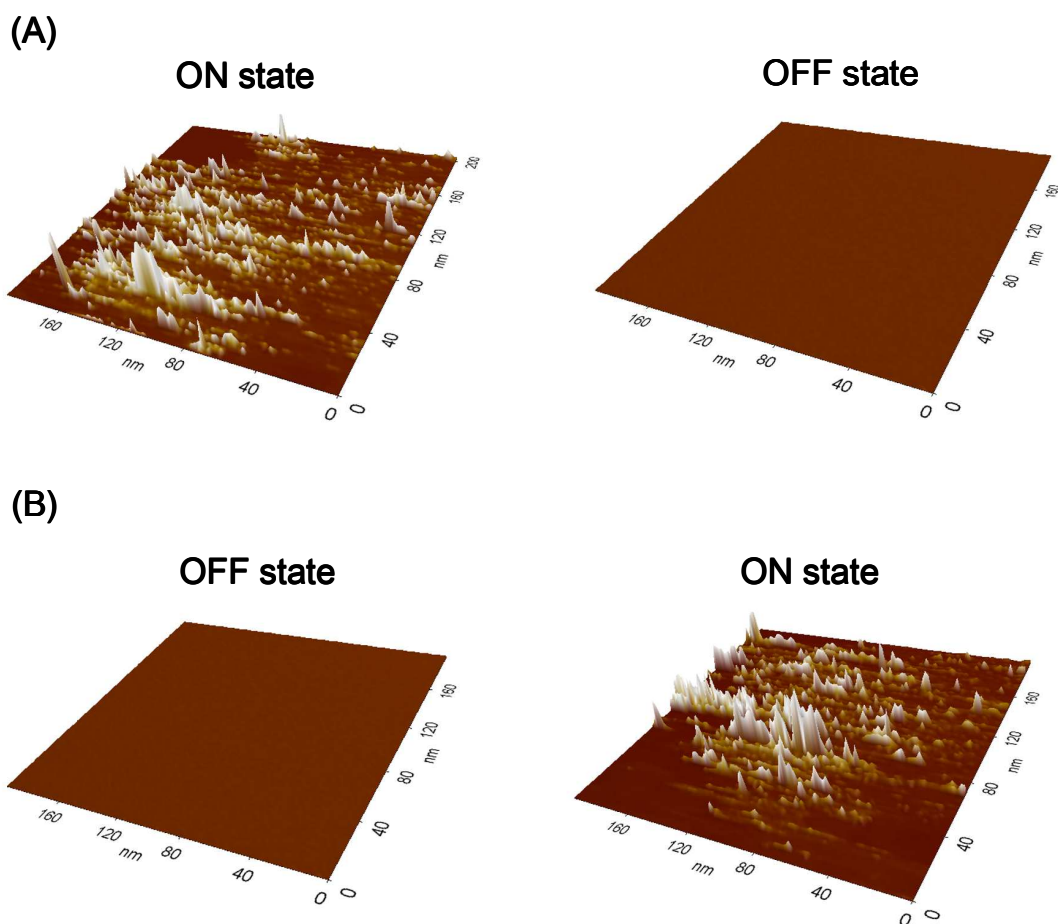
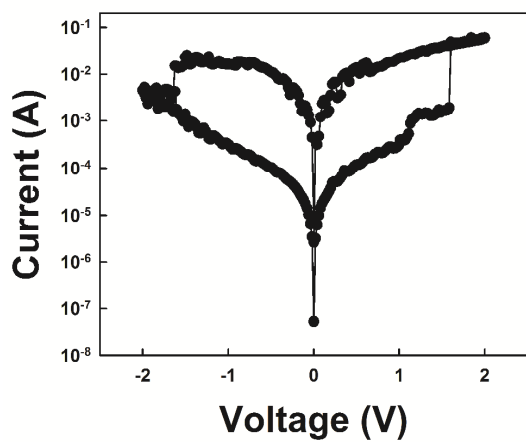
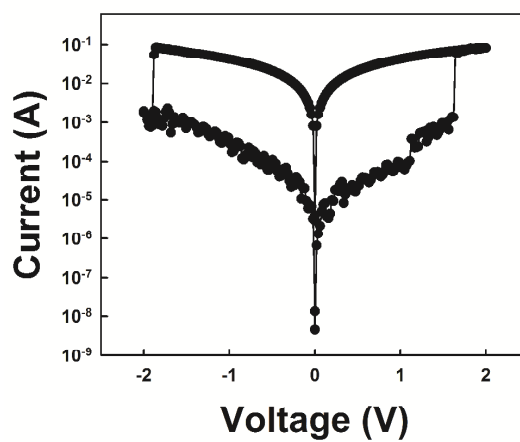


**Figure S10.** CS-AFM images of  $(\text{NH}_2\text{-dendrimer/OA-BTO NP})_5$  multilayers in ON ( $\sim -6$  V) and OFF state ( $\sim -0.2$  V) during (A) negative voltage sweep, and OFF ( $\sim +0.2$  V) and ON ( $\sim +6$  V) state during (B) positive voltage sweep, respectively. CS-AFM images of multilayer devices were measured from the respective regions in  $I$ - $V$  curve of  $(\text{NH}_2\text{-dendrimer/OA-BTO NP})_3$  multilayer device. The formation of conductive filamentary paths was confirmed by CS-AFM characterizations. In this case, electrochemically inert Pt tip was used as a top electrode instead of Ag electrode. The formation and rupture of the randomly distributed paths were observed after “SET” processes (*i.e.*, switching from low current (OFF) to high current (ON) state) and “RESET” (*i.e.*, switching from high current (ON) to low current (OFF) state).

(A)



(B)



(C)

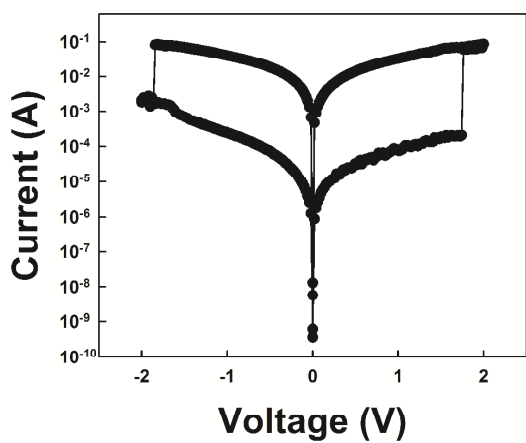


**Figure S11.**  $I$ - $V$  curves of  $(\text{NH}_2\text{-dendrimer/OA-BTO NP})_5$  multilayer devices measured from (A) Au, (B) Pt, and (C) W top electrodes.